Journal of *Marine Science and Engineering*

MDPI

Article

Dynamic Evolution Mechanisms and Lateral Spreading Prediction of Coral Sand Particle Clouds in Still Water

Jie Chen [1,2,3,*], Feifei Li [1], Xueying Liu [1], Changbo Jiang [1,2,3], Zhiyuan Wu [1,2,3] and Zhen Yao [1,4]

[1] School of Hydraulic and Ocean Engineering, Changsha University of Science & Technology, Changsha 410114, China; stronggirl@csust.edu.cn (F.L.); trip_linker@163.com (X.L.); jiangchb@csust.edu.cn (C.J.); zwu@csust.edu.cn (Z.W.); yaozhen@zuwe.edu.cn (Z.Y.)
[2] Key Laboratory of Water-Sediment Sciences and Water Disaster Prevention of Hunan Province, Changsha 410114, China
[3] Key Laboratory of Dongting Lake Aquatic Eco-Environmental Control and Restoration of Hunan Province, Changsha 410114, China
[4] Zhejiang Key Laboratory of River-Lake Water Network Health Restoration, Hangzhou 310018, China
* Correspondence: chenjie166@163.com

Abstract

Coral sands are critical in the construction of islands and harbors in tropical regions. Studying their dispersal, specifically the movement of 'sedimentary clouds' during marine dumping/dredging operations, is essential for optimizing construction efficiency and mitigating impacts on marine ecosystems. This study investigates the evolutionary characteristics of coral sand particles in still water via controlled indoor experiments. By manipulating parameters such as particle size, mass, nozzle diameter, and air release height, this study evaluated the impact of aspect ratio, Stokes number, and initial particle momentum on the movement of coral sand clouds. The results indicate that variations in air release height modulated the cloud's width and corresponding diffusion angle, but exerted a negligible impact on the cloud front's velocity and position. Empirical formulas for traditional quartz sand have limitations in reflecting the complex hydrodynamic settling behavior of coral sand. To address this, this paper establishes a modified empirical equation. This equation effectively predicts the width of coral sand plumes across different air release heights and Stokes number ranges. Furthermore, rather than directly quantifying microscopic morphological features, this study interprets these macroscopic transport characteristics from a process-based hydrodynamic perspective. Ultimately, the resulting predictive data and empirical framework provide a practical reference for evaluating sediment dispersion in reef engineering projects.

Keywords: coral sand; particle clouds; particle shape; release height; diffusion; predictive model

Check for updates

Academic Editor: Juan J. Munoz-Perez

Received: 2 June 2026
Revised: 27 June 2026
Accepted: 28 June 2026
Published: 2 July 2026

Copyright: © 2026 by the authors. Licensee MDPI, Basel, Switzerland. This article is an open access article distributed under the terms and conditions of the Creative Commons Attribution (CC BY) license.

1. Introduction

Recently, land reclamation has become a primary strategy for many coastal regions. It effectively addresses the growing demand for habitable and industrial land [1–3]. Among the most prominent examples is the hydraulic fill engineering undertaken in the South China Sea [4]. However, while land reclamation extends usable territory, it severely damages fragile coral reef ecosystems [5]; the dispersion of suspended sediments and the burial of benthic organisms caused by sand dumping have led to significant degradation of the marine environment [6]. Understanding the hydrodynamic evolution and transport

mechanisms of fill materials is imperative. These insights are essential for modeling coastal impacts and refining reclamation designs [7].

However, land reclamation operations inevitably generate sediment plumes. The movement and dispersion of these plumes can result in significant material loss and displacement of the placement point [8,9]. This necessitates extensive subsequent earthwork adjustments, severely disrupting the construction schedule and thereby significantly reducing operational efficiency [10]. To gain a deeper understanding of the dynamic mechanisms underlying sediment dispersion, research efforts should focus on the physical process by which sediment is released into the water instantaneously in the form of a "particle cloud" [11–13].

The sedimentation dynamics of particle clouds are typically delineated into three distinct kinetic phases. Acceleration regime: The cloud accelerates downward as its submerged weight overcomes hydrodynamic drag [14]. Thermal regime: The cloud settles as a cohesive entity, continuously entraining ambient water and transferring momentum. Dispersion regime: As the cloud's bulk momentum dissipates, collective effects collapse. Particles decouple from the cloud, transitioning to independent settling at their respective terminal velocities (u_∞) [15,16].

Notably, unlike land reclamation projects on the mainland, those in the South China Sea primarily use coral sand as the main fill material, resulting in the formation of coral-sand islands [17]. From a mineralogical perspective, coral sand is a calcareous sediment derived from fragments of marine skeletons, and its physical and mechanical behavior differs fundamentally from that of traditional quartz sand [18–20]. Early morphological classifications—categorizing particles as blocky, platy, branched, or rod-shaped—laid the foundation for understanding grain geometry [21]. Recent studies have shown that coral sand exhibits particle fragility [22], as well as irregular shapes, high specific surface area, and abundant skeletal pores [23,24]. These complex configurations and porous structures are widely recognized as significantly influencing particle–fluid interaction mechanisms, particularly the hydrodynamic resistance response [25,26]. Therefore, the direct application of classical mechanical models and empirical equations based on quartz sand to coral sand may have limited applicability [22,27–31]. Recognizing these differences, numerous researchers have investigated the key hydrodynamic variables that govern the evolution of such particle clouds.

Previous studies have conducted systematic research on the key controlling variables of particle clouds. The initial geometric boundary conditions are the core driving force for the macroscopic evolution. The research results of Azimi et al. show that variables such as nozzle diameter, aspect ratio, and distance between dual nozzles fundamentally determine the evolution of the front, the maximum diffusion width, and the formation of clusters [10,32–35].

Particle size and the Stokes number are equally critical to microfluidic behavior, influencing fluid entrainment capacity and mixing efficiency, and ultimately regulating cluster effects and the evolution of internal turbulence [36]. Furthermore, the release height determines the system's initial potential energy, which, in combination with the ambient hydrodynamic conditions, strongly influences the initial acceleration, trajectories, and final settling velocity of particle clusters [32,33,37].

However, the fundamental assumption of idealized particle morphology severely limits the applicability of existing theoretical models. Furthermore, the current literature largely lacks a systematic coupling logic between initial control variables and the evolution of macroscopic particle clouds; previous studies have mostly been limited to evaluating the impact of a single variable. This has resulted in the continued absence of a comprehensive multivariate mapping framework. Although the unique drag characteristics of

coral sand have been recognized [38], systematic theoretical support regarding how key variables—particle size, release height, nozzle diameter, and Stokes number (St)—interact to control the position and velocity of the front, cloud width, and diffusion angle of the front remains lacking. These limitations underscore the need for systematic experiments on the macroscopic multiparameter hydrodynamics of coral sand.

Based on the aforementioned theoretical gaps and practical engineering needs, this paper systematically investigates the dynamic evolution mechanisms of coral sand particle clouds in still water. Rather than directly quantifying microscopic morphological differences, this study aims to elucidate macroscopic transport characteristics. The main research objectives and scientific contributions are as follows:

Elucidation of macroscopic hydrodynamic mechanisms: The sedimentation velocity, kinematic characteristics, and dispersion patterns of coral sand clouds were systematically measured. This approach contributes systematic experimental data to the multiphase flow dynamics of complex natural sediments and provides macroscopic observations that extend current empirical relationships.

Establishing a multivariate coupled framework: Initial boundary conditions (particle size, air release height, and nozzle diameter) were systematically controlled. The interactive effects of the initial aspect ratio (L_0/d_0), the Stokes number (St), and initial kinetic energy on cloud evolution were thoroughly analyzed. This framework elucidates the multi-parameter driving mechanisms.

Development of a predictive empirical model: Based on the experimental dataset, a modified semi-empirical model was established. This model effectively predicted the diffusion width of coral sand particle clouds. Furthermore, diffusion coefficients were calculated, providing practical, data-driven support for subsequent macroscopic engineering simulations.

2. Material and Methods

2.1. Experimental Setup

The experiment was conducted in the Hydraulic Engineering Laboratory of Changsha University of Science and Technology. This study aims to explore the evolution process of coral sand particle clouds under static water conditions. The experimental setup and coordinate system are shown in Figure 1. The main tank measured 1.4 m in length, 0.5 m in width, and 0.8 m in depth. The side walls and bottom of the water tank are made of transparent acrylic glass to meet the requirements of optical observation. The sand and stone release device is fixed above the center of the water tank. The bottom of the device is equipped with a sliding baffle controlled by an electromagnetic valve. This design enables the instantaneous release of sand and stones, minimizing the disturbance to the still water surface and the surrounding environment. During the experiments, the water depth in the tank was maintained at 0.8 m. The water temperature was maintained at 24 ± 1 °C, with a fluid density of 1000 kg/m^3 and a dynamic viscosity of 1.247×10^{-3} Pa·s. There are abundant pores inside the coral sand particles. To eliminate the interference of escaping bubbles during the sedimentation process on the flow field, all test samples were soaked in water for 24 h before the experiment to achieve complete saturation.

The experimental material consisted of natural coral sand sediments collected in situ, with a particle skeletal density (solid density) of 2780 kg/m^3. The sand samples were sieved using vibrating screens with mesh sizes ranging from 0.105 mm to 0.9 mm. After screening, four sets of sand samples were obtained with median particle sizes (D_{50}) of 0.178 mm, 0.350 mm, 0.580 mm, and 0.805 mm, respectively. These four particle size groups were selected because they accurately represent the typical coral sand size distributions widely used in actual marine land reclamation projects. Additionally, the Stokes number (St) is

a key dimensionless parameter influencing particle motion [39]. Each particle size group corresponds to a different Stokes number range: for small particles with D_{50} = 0.178 mm, the St range is [0, 0.1]; for medium particles with D_{50} = 0.350 mm, the St range is [0.1, 0.33]; for large particles with D_{50} = 0.580 mm and 0.805 mm, the St range is [0.33, 1]. The St range selected here effectively covers the key hydrodynamic transition stages during the evolution of the particle cloud. This coverage ensures that subsequent analyses are firmly grounded in the actual physical and engineering context.

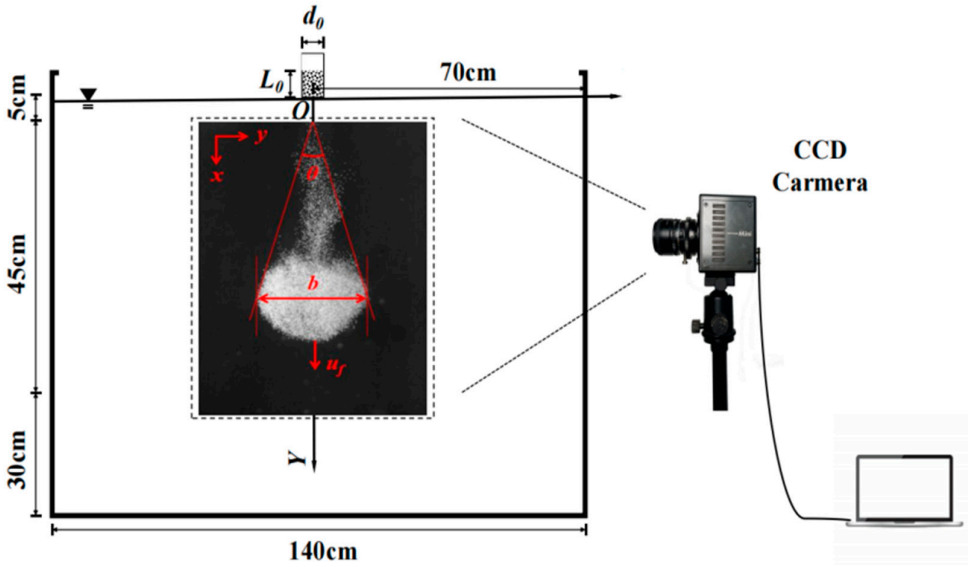


Figure 1. Experimental setup for monitoring the evolution of coral sand clouds using a CCD camera (coral sand released into the monitoring area from a fixed height).

The experiment was conducted in a darkroom environment. A 150 W tricolor soft light was used as the light source. Black opaque cloth was hung behind the tank to eliminate light reflection from the background wall and enhance image contrast. As shown in Figure 1, a high-speed camera (MEMRECAM HX-7S nac Image Technology, Tokyo, Japan) was used to fully record the evolution of the coral sand cloud. The camera's optical axis was aligned directly with the center of the aquarium's side wall and maintained in strict vertical alignment to eliminate perspective distortion in the images (Figure 1). The camera was equipped with an AF 50 mm $f/1.8$ DI fixed-focus lens (Nikon, Tokyo, Japan), with a resolution of 2560 × 1920 pixels. Raw images were recorded at a frame rate of 250 frames per second, and the camera was calibrated using the MATLAB 2022b toolbox 'Camera Calibrator'. To ensure experimental accuracy, preliminary tests were conducted in the tank.

A total of 52 experimental runs were conducted. To ensure comprehensive coverage of the parameter space and to accurately investigate the effect of a single variable, the experiments employed a strict controlled-variable design. The experiments were divided into three series. In Series A (A1–A24), the release height (H = 0) was kept constant, and the effects of the aspect ratio (L_0/d_0) and the Stokes number (St) were analyzed by varying the initial sand mass (m) and particle size (D_{50}). To analyze the effect of release height, Series B (B1–B14) and Series C (C1–C14) maintained the same combinations of initial conditions as Series A, but adjusted the release height to H = 10 and H = 20, respectively. The detailed parameters for all 52 test conditions are summarized in Table 1. The interval between each consecutive experiment was strictly controlled to be more than 10 min to ensure that the water in the tank completely returned to a static state. After each experiment, the deposited sand particles at the bottom of the tank were immediately removed. This procedure prevented changes in water depth caused by the elevation of the bed. The water

surface elevation and the spatial coordinates of the release device were kept absolutely constant throughout all tests, ensuring uniform boundary conditions.

Table 1. Experimental details of the coral sand particle clouds in water with different Combinations of initial conditions.

Test	D_{50} (mm)	d_0 (mm)	m (g)	H (cm)	L_0/d_0	u_∞ (m/s)	F_B (10^{-5}) (m^4/s^2)	St	η
A1	0.805	15	4	0	0.905	0.188	1.41	0.894	1
A2		15	8	0	1.810		2.82	0.894	1
A3		15	12	0	2.715		4.23	0.894	1
A4		15	16	0	3.621		5.65	0.894	1
A5		20	4	0	0.382		1.41	0.774	1
A6		20	16	0	1.527		5.65	0.774	1
A7	0.580	15	4	0	0.905	0.098	1.41	0.464	1
A8		15	8	0	1.810		2.82	0.464	1
A9		15	12	0	2.715		4.23	0.464	1
A10		15	16	0	3.621		5.65	0.464	1
A11		20	4	0	0.382		1.41	0.402	1
A12		20	16	0	1.527		5.65	0.402	1
A13	0.350	15	4	0	0.905	0.036	1.41	0.169	1
A14		15	8	0	1.810		2.82	0.169	1
A15		15	12	0	2.715		4.23	0.169	1
A16		15	16	0	3.621		5.65	0.169	1
A17		20	4	0	0.382		1.41	0.146	1
A18		20	16	0	1.527		5.65	0.146	1
A19	0.178	15	4	0	0.905	0.009	1.41	0.043	1
A20		15	8	0	1.810		2.82	0.043	1
A21		15	12	0	2.715		4.23	0.043	1
A22		15	16	0	3.621		5.65	0.043	1
A23		20	4	0	0.382		1.41	0.038	1
A24		20	16	0	1.527		5.65	0.038	1
B1	0.805	15	8	10	1.810	0.188	2.82	0.894	5.46
B2		20	16	10	1.527		5.65	0.774	4.76
B3	0.580	15	4	10	0.905	0.098	1.41	0.464	5.46
B4		15	8	10	1.810		2.82	0.464	5.46
B5	0.350	15	16	10	3.621	0.036	5.65	0.464	5.46
B6		20	16	10	1.527		5.65	0.402	4.76
B7		15	4	10	0.905		1.41	0.169	5.46
B8		15	8	10	1.810		2.82	0.169	5.46
B9		15	16	10	3.621		5.65	0.169	5.46
B10		20	16	10	1.527		5.65	0.146	4.76
B11	0.178	15	4	10	0.905	0.009	1.41	0.043	5.46
B12		15	8	10	1.810		2.82	0.043	5.46
B13		15	16	10	3.621		5.65	0.043	5.46
B14		20	16	10	1.527		5.65	0.038	4.76
C1	0.805	15	8	20	1.810	0.188	2.82	0.894	7.66
C2		20	16	20	1.527		5.65	0.774	6.65
C3	0.580	15	4	20	0.905	0.098	1.41	0.464	7.66
C4		15	8	20	1.810		2.82	0.464	7.66
C5		15	16	20	3.621		5.65	0.464	7.66
C6		20	16	20	1.527		5.65	0.402	6.65
C7	0.350	15	4	20	0.905	0.036	1.41	0.169	7.66
C8		15	8	20	1.810		2.82	0.169	7.66
C9		15	16	20	3.621		5.65	0.169	7.66
C10		20	16	20	1.527		5.65	0.146	6.65

Table 1. *Cont.*

Test	D_{50} (mm)	d_0 (mm)	m (g)	H (cm)	L_0/d_0	u_∞ (m/s)	F_B (10^{-5}) (m^4/s^2)	St	η
C11	0.178	15	4	20	0.905	0.009	1.41	0.043	7.66
C12		15	8	20	1.810		2.82	0.043	7.66
C13		15	16	20	3.621		5.65	0.043	7.66
C14		20	16	20	1.527		5.65	0.038	6.65

2.2. Image Processing and Data Extraction

An advanced image processing technique was developed using the MATLAB Image Processing Toolbox [40] to accurately characterize the dynamics of coral sand particle clouds. This technique enables the precise extraction of relevant kinematic data by effectively separating the coral sand clouds from the background.

First, the experimentally acquired RGB images were converted into grayscale matrices to reduce data dimensionality. Grayscale conversion transforms chromatic information into intensity values, facilitating the identification and isolation of regions of interest. To eliminate static background noise and enhance the visibility of the particle cloud, a sliding background subtraction algorithm was employed [40]. This process subtracts the grayscale values of the static background image from those of transient experimental image; its mathematical expression [32] can be represented as follows:

$$I_{diff}(x,y,t) = \left| I_{esp}(x,y,t) - I_{bg}(x,y,t) \right| \quad (1)$$

Subsequently, the front velocity (u_f), front position (x), cloud width (b), and diffusion angle (θ) of the particle cloud were precisely determined using multi-pixel value search technology. This method, similar to that employed by Azimi et al. [32], detects boundaries by systematically searching pixel values, thereby accurately identifying the characteristic boundaries of the particle cloud. The multi-pixel value search technique ensures the accuracy and reliability of the extracted spatial features, providing a robust foundation for subsequent analysis.

In addition, this study examined the uncertainty of the experimental data using operating condition A8 (D_{50} = 0.580 mm, L_0/d_0 = 1.810) as a representative example. This operating condition was selected because its parameters represent the median values across the entire experimental range. The test was repeated four times to quantify its repeatability. Since the exact same optical setup, spatial resolution, and multi-pixel boundary detection algorithm were strictly applied across all 52 experimental sets, the derived uncertainty estimates are considered highly representative of the entire experimental series. The results show that for the front velocity (u_f), front position (x), cloud width (b), and diffusion angle (θ), the maximum measurement uncertainties are ±1%, ±2%, ±9%, and ±5%, respectively.

3. Results and Discussion

3.1. Evolution of the Coral Sand Clouds

The complex interaction between gravity settling and diffusion governs the evolution process of particle clusters released into water bodies. To quantify the dynamic evolution process of coral sand clouds in still water, this study draws on previous theories [39] and introduces dimensionless time t^*. The initial moment when particles are released into the water is defined as t^* = 1. High-speed imaging technology captured the specific process of the experiment, along with precise measurement and tracking of the morphology of the particle cloud.

This section analyzes a specific condition with a median particle diameter (D_{50}) of 0.805 mm and a fixed release height (H) of 0 cm. Figure 2 shows the evolution process of the particle cloud under four dimensionless times (t^* = 1, 6, 12, 20). At t^* = 1, the instantaneous release of particles generated a high-density cloud at the release point. The more obvious trailing stem is a typical feature of this stage. As the particles descend, this trail gradually decays. Subsequently, the mixing of the cloud tail and the front marks the thermal bubble period of the particle cloud, the beginning of the Thermal regime [14]. Crucially, this phase transition is not limited to visual observation alone; it is quantitatively supported by a marked deceleration in the front velocity (u_f) and a rapid lateral expansion of the cloud width (b), as will be clearly demonstrated in Section 3.2 and subsequent analyses. When t^* = 6, the particle cloud experienced greater dispersion. This dispersion marks the beginning of gravity settling and diffusion. These two driving forces together shape the evolving cloud [41]. The kinematic evolution curve described in detail below provides further mathematical support for this dynamic equilibrium. At t^* = 12, the cloud expands further, and the continuous sedimentation and dispersion of particles in the water tank accelerate this process, while reflecting the dominance of the gravity-diffusion mechanism.

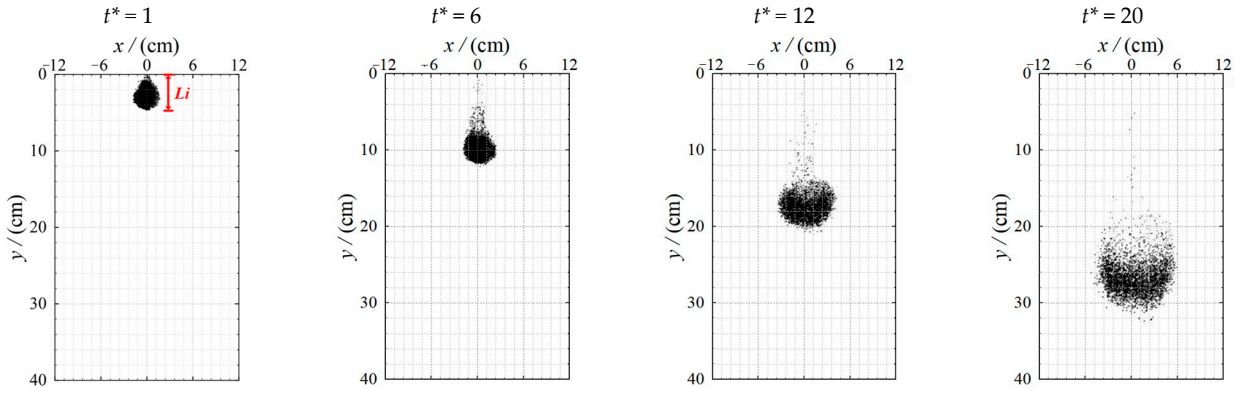


Figure 2. Effect of particle size on the evolution of particle clouds for L_0/d_0 = 0.382 and at different non dimensional time scales, t^*; D_{50} = 0.805 mm.

Finally, at t^* = 20, the particle cloud reaches the swarm phase [39], a relatively stable state. The wider spatial distribution and lower concentration characterize this final stage. This indicates that a balance has been reached between the gravity settling and diffusion processes.

In order to analyze the dynamic mechanism during the evolution process of the particle cloud more precisely, this study introduces the characteristic length (L_i) proposed by Moghadaripour et al. [39]. At $x = L_i$, it is considered as the beginning of the transient particle cloud (as shown in Figure 2 at t^* = 1), and x represents the distance between the particle cloud front and the water surface. Figure 3 presents the trajectory of the normalized pre-front position (x/L_i) as a function of dimensionless time (t^*), which further illustrates the evolution law of the particle cloud. This trajectory clearly delineates the three stages of the particle cloud evolution.

In region I ($t^* \leq 1$), the cloud shows significant characteristics of sand jet flow. The empirical formula proposed by Azimi et al. [32] can accurately predict the dynamic behavior in this region. As the normalized pre-front position (x/L_i) increases with dimensionless time (t^*), it indicates that the front edge of the cloud has a higher initial velocity during this period. Region II ($1 < t^* < 6$)) represents the transition of the system from the initial acceleration period to the thermal phase (Thermal phase). The nonlinear relationship between the normalized pre-front position (x/L_i) and dimensionless time (t^*) constitutes a significant feature of this stage. In region III ($t^* \geq 6$), the particle cloud enters the thermal

state. The front speed decreases with time and the lateral expansion of the cloud, which is a core feature of this stage [42]. Notably, the transition to the hot state was not merely inferred from the trajectory of x/L_i, but was verified using the data from Section 3.2, which was obtained based on quantitative velocity decay measurements.

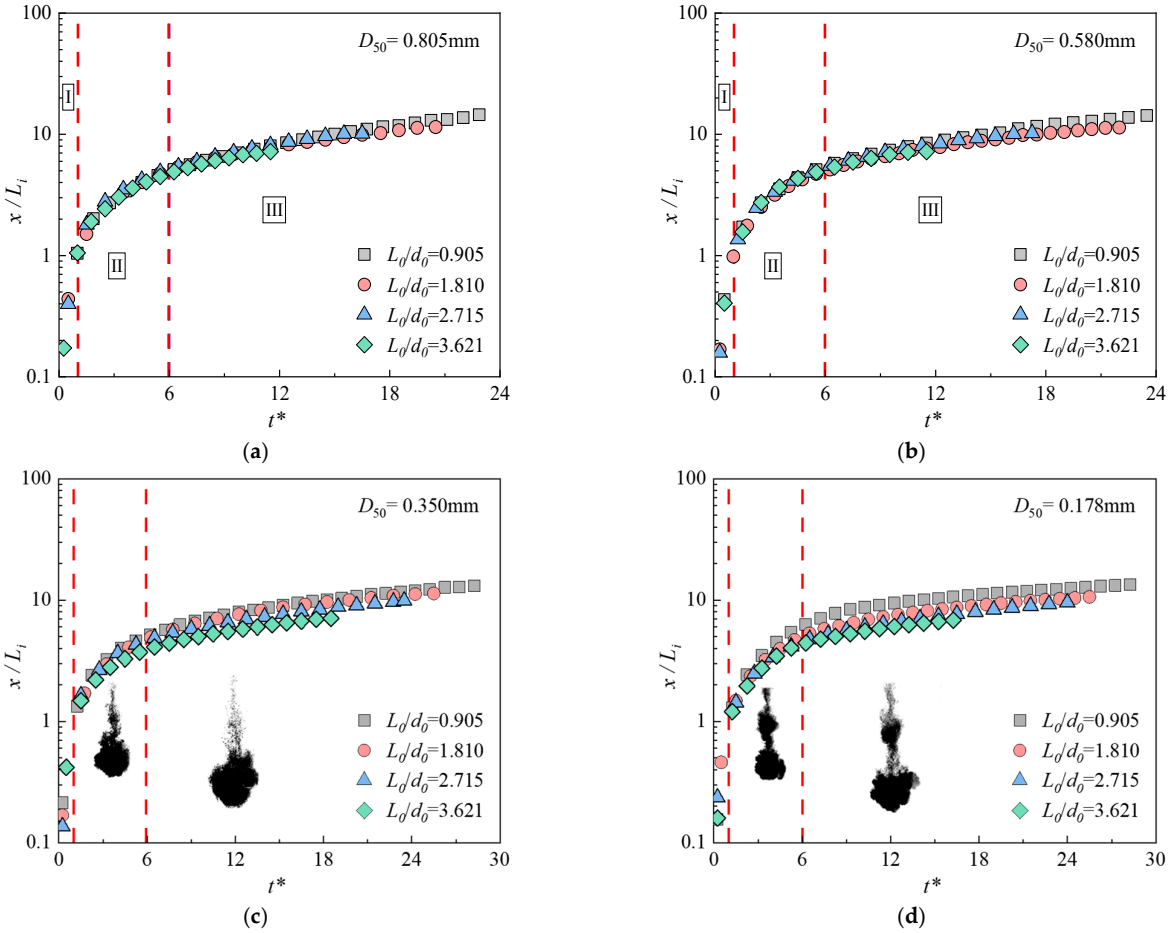


Figure 3. Variations in the normalized frontal position, x/L_i, with the nondimensional time, t^*. (**a**) Results for particle size D_{50} = 0.805 mm; (**b**) Results for particle size D_{50} = 0.580 mm; (**c**) Results for particle size D_{50} = 0.350 mm; (**d**) Results for particle size D_{50} = 0.178 mm. The vertical red dashed lines demarcate the three evolutionary stages (I, II, and III). The inset images illustrate the typical macroscopic morphology of the coral sand clouds taken at t^* = 6 and t^* = 12.

For particle clouds composed of medium and small-sized particles (Figure 3c,d), within the range of $1 < t^* < 12$, particle clouds with a "tail stem" structure can be observed. As the cloud further sinks, the tail gradually merges with the front, resulting in the enlargement of the cloud ladder. Eventually, based on the classification system proposed by Bühler and Papantoniou [43], coral sand particle clouds officially enter the swarm phase at $t^* = 20$.

Based on dimensionless time (t^*), the evolution of coral sand clouds can be classified into three distinct phases. In the initial jet phase ($t^* \leq 1$), an extremely high initial velocity and the trailing stem constitute the defining transient characteristics. Subsequently ($1 < t^* < 6$), trailing stem merger drives a nonlinear morphological transition. Upon entering the thermal phase ($t^* \geq 6$) [39], fluid entrainment leads to frontal velocity attenuation and lateral expansion. This transition, along with the equilibrium reached between gravitational settling and turbulent dissipation at $t^* = 20$ [44], no longer depends entirely on the evolution of position but is strongly supported by the independent kinematic evidence (front velocity) provided in Section 3.2. This equilibrium marks the complete transition of the particle cloud to a stable collective settling phase.

3.2. Frontal Velocity

This section assesses the effects of release height, aspect ratio, and particle size on the velocity of the coral sand cloud front. Based on the image processing work, the front velocity (u_f) is defined as the ratio of the cloud front displacement to the time step ($u_f = \Delta x/\Delta t$). Here, the time step (Δt) is determined by the reciprocal of the sampling frame rate (fps) of the high-speed camera. Additionally, the final settling velocity of a single particle (u_∞) is controlled by Stokes' law. This theory is expressed as $u_\infty = g(\rho_s - \rho_w)D_{50}^2/18\mu$, where ρ_s and ρ_w respectively refer to the density of the coral sand particles and the water body, and is the dynamic viscosity coefficient of the fluid.

The air release height (H) determines the initial momentum of the particle cluster at the moment of entering the water. To quantify the influence of the release height (H) on the front velocity, this section fixes the aspect ratio as L_0/d_0 = 1.810 and compares and analyzes the evolution of the coral sand cloud under three release heights (H = 0, 10, 20 cm) with different particle size distributions (Figure 4). As shown in Figure 4, the initial settling velocity increases with the increase in release height. However, as the normalized depth (x/d_0) increases, the normalized front velocity (u_f/u_∞) converges rapidly under different release heights. This phenomenon indicates that the influence of the air release height (H) on the particle cloud front velocity is negligible.

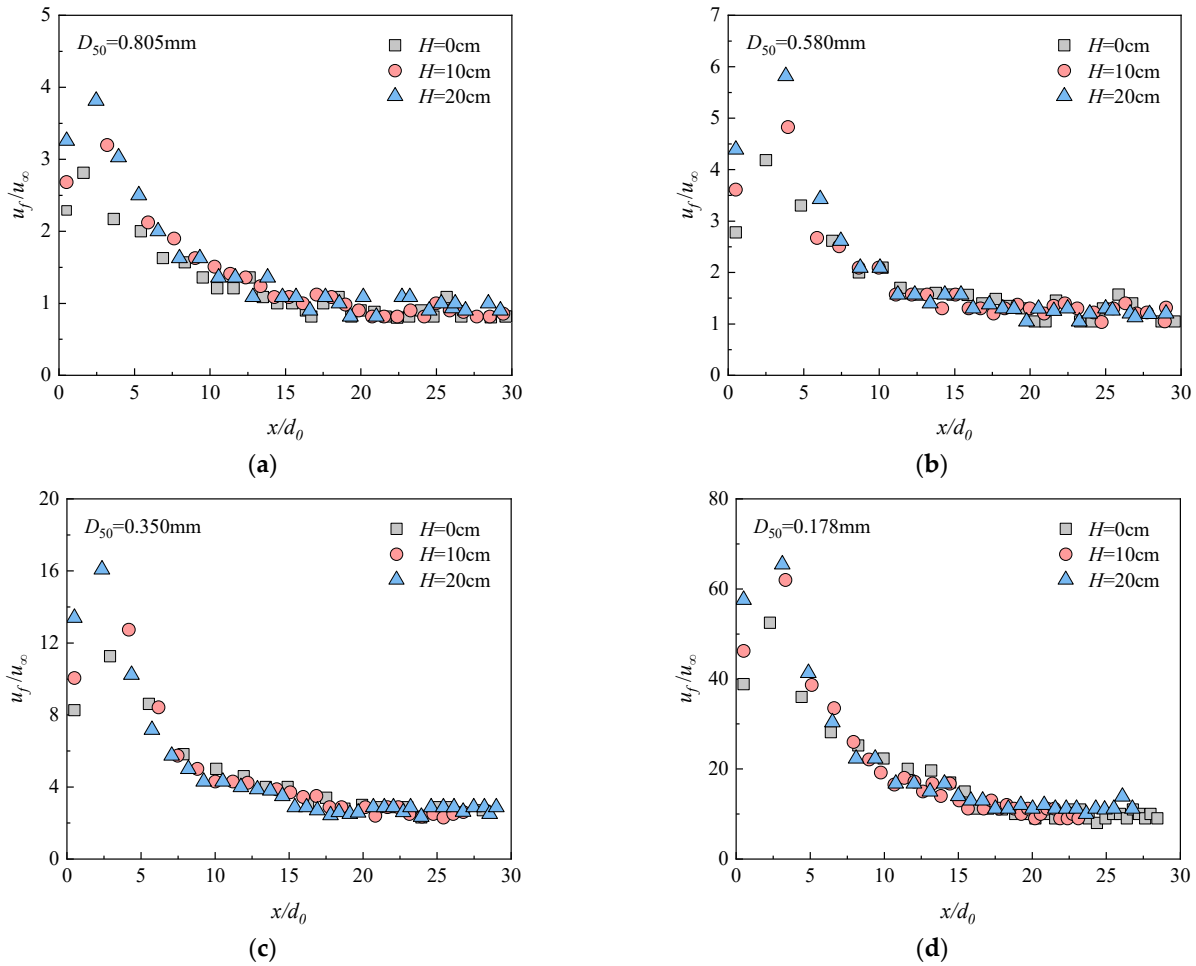


Figure 4. Effect of air release height on normalized velocity, u_f/u_∞, of particle clouds with different particle sizes: L_0/d_0 = 1.810. (**a**) Results for particle size D_{50} = 0.805 mm; (**b**) Results for particle size D_{50} = 0.580 mm; (**c**) Results for particle size D_{50} = 0.350 mm; (**d**) Results for particle size D_{50} = 0.178 mm.

The effects of aspect ratio and particle size on the front velocity of a coral sand cloud were investigated at an air release height of H = 0 cm (Figure 5). The normalized front velocity of the particle cloud decreased with increasing depth. This trend is consistent with the observations reported in [45]. In general, a larger aspect ratio results in a higher initial front velocity and a higher normalized terminal settling velocity for the particle cloud.

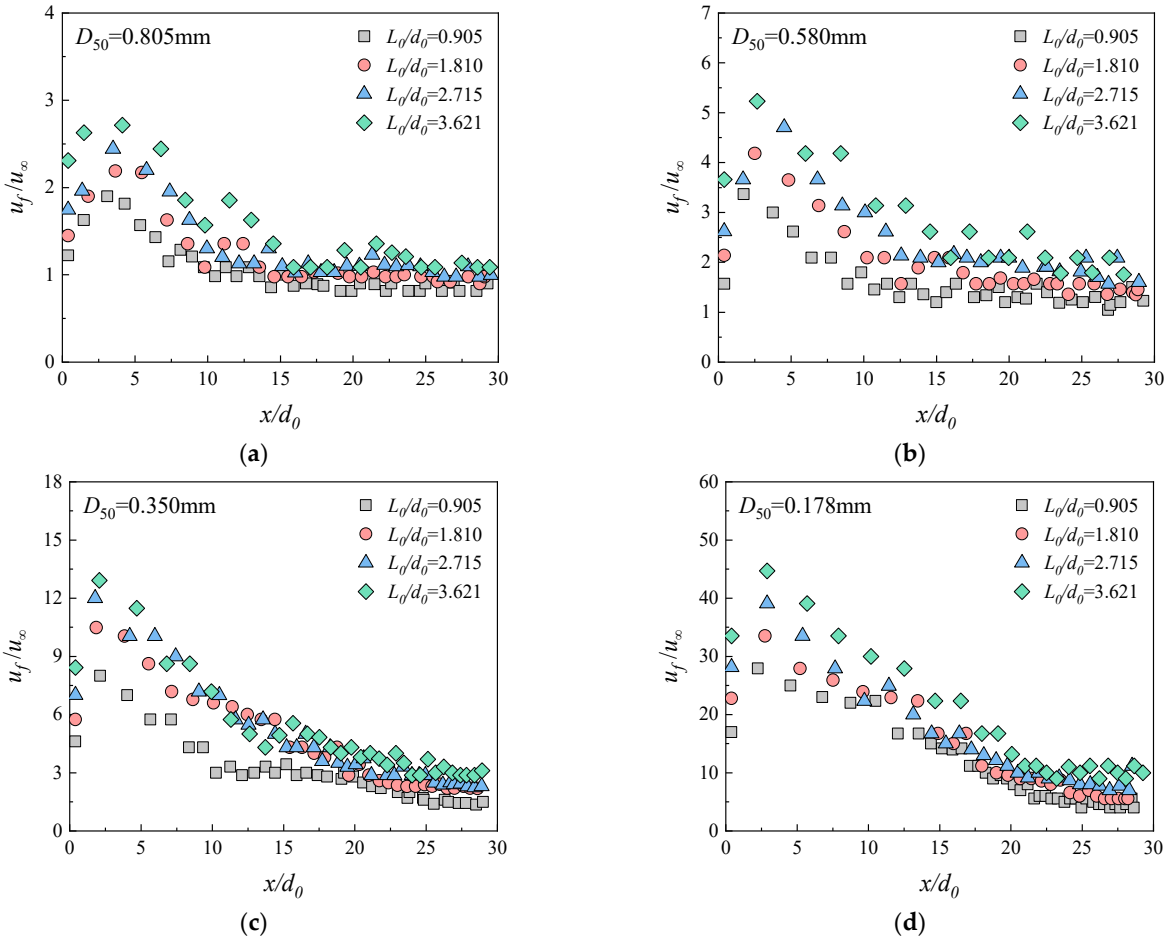


Figure 5. Variations in the frontal velocity with time for different median particle sizes. (**a**) Results for particle size D_{50} = 0.805 mm; (**b**) Results for particle size D_{50} = 0.580 mm; (**c**) Results for particle size D_{50} = 0.350 mm; (**d**) Results for particle size D_{50} = 0.178 mm.

Figure 6 reveals the influence of varying initial aspect ratios (L_0/d_0) on the evolution of the normalized frontal velocity (u_f/u_∞) of coral sand. The collective acceleration observed during the initial settling stage primarily originates from inter-particle collective effects. For analogous processes, Moghadaripour et al. [39] established an empirical formula for quartz sand diffusion (Equation (2)):

$$\frac{u_f}{u_\infty} = \phi\left[\frac{x}{d_0}\left(\frac{L_0}{d_0}\right)^{\lambda}\right]^{\xi} \quad (2)$$

where φ, λ, and ξ are empirical coefficients with values of 9.4, −0.61, and −0.5, respectively. However, quantitative performance metrics indicate that applying Equation (2) directly to the current coral sand data yields significant discrepancies, characterized by a root-mean-square error (RMSE) as high as 5.62 and an extremely low coefficient of determination (R^2) of 0.34. Deviations of this magnitude are due to the fact that Equation (2) neglects the key effects of particle size and intrinsic morphology.

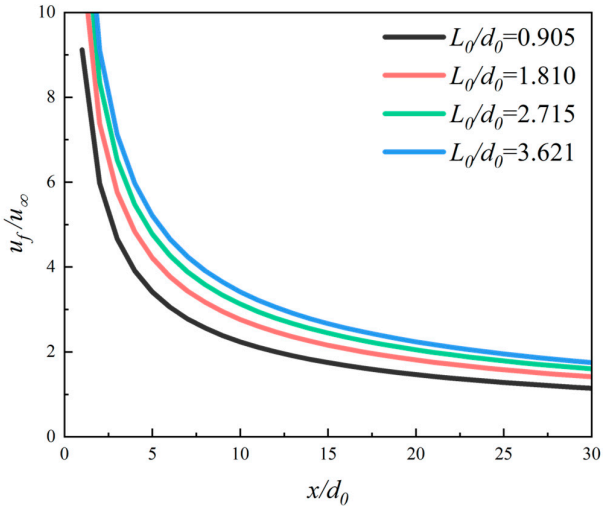


Figure 6. Variability in coral sand frontal velocities at different aspect ratios.

Figure 6 shows that the normalized frontal velocity of coral sand decreases nonlinearly with the increase in the dimensionless distance (x/d_0). The initial aspect ratio is larger, the initial frontal velocity will be greater. When x/d_0 exceeds 10, the linear change gradually converges, and the frontal velocity eventually stabilizes in a lower range. These results indicate that the previous empirical formulas are not applicable to coral sand and the relevant parameters need to be modified.

The Stokes number is introduced here because a larger grain size corresponds to greater irregularity in individual coral sand particles. To characterize the shape of coral sand, Chen et al. [23] defined the shape factor SF_{50} as the cumulative shape factor distribution percentage corresponding to the median particle size D_{50} reaching 50%, representing the form factor under the same D_{50}.

$$St = \frac{\tau_P}{\tau_f} = \frac{(\rho_s - \rho_w) D_{50}^2 u_0}{18 \mu d_0} \tag{3}$$

where $\tau_P = \frac{(\rho_s - \rho_w) D_{50}^2}{18\mu}$, $\tau_f = \frac{d_0}{u_0}$.

Figure 7 shows the differences in the cloud front velocities of coral sand with different particle sizes under the same aspect ratio (L_0/d_0 = 1.810). The smaller the particle size, the greater the normalized cloud front velocity of the particle cloud (Figure 7). For small particle sizes ($0.1 < St \leq 0.33$), the normalized cloud front velocity of the particle cloud (u_f/u_∞) decreases with the decrease in the normalized cloud front position (x/d_0) and eventually stabilizes. For $0.33 < St < 1$ (i.e., medium and large particle sizes), the changes in the particles are not very obvious. Figure 7 shows that the particles tend to fall separately and the velocity remains basically unchanged within a short period of time. This conclusion is similar to that of quartz sand [39]. However, Chen et al. [41] found that the cloud front velocity of coral sand in water is smaller than that of quartz sand. Under the same conditions, the coral sand particles are subject to greater resistance in water. It is crucial to recognize that grain size and microshape vary simultaneously in natural coral sand sediments. Therefore, the significant differences in flow velocity observed among different D_{50} groups (Figure 7) cannot be attributed to shape factors in isolation. Rather, they represent the complex coupled contributions of both grain size and its inherent, grain-size-dependent morphological characteristics.

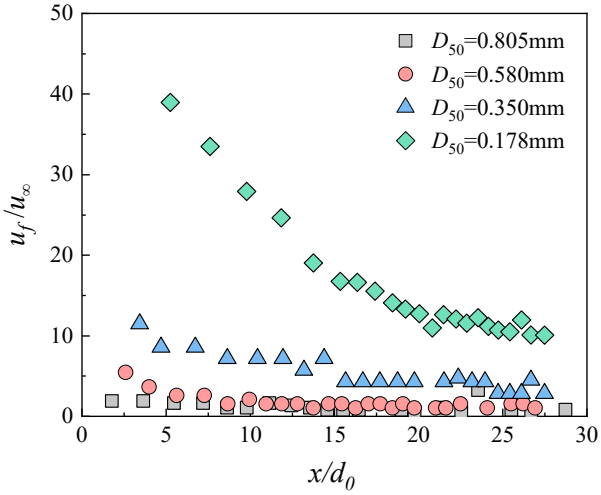


Figure 7. Variations in frontal velocities of particle clouds with different median particle sizes (*D50*), at the same aspect ratio, L_0/d_0 = 1.810.

To uncover the physical laws underlying the observed phenomena, it is necessary to consider hydrodynamics based on physical processes. The rapid convergence and decay of the front velocity (u_f/u_∞) can be explained by the following mechanisms. Unlike smooth, spherical quartz sand, the irregularity and complex pore structure of coral sand particles alter the interaction mechanisms between the fluid and the particles.

Due to their honeycomb-like skeletal pores and rough, non-spherical surfaces, coral sand particles exhibit higher drag than conventional sediment, leading to intense momentum dissipation immediately upon entry into the water [41,46]. Furthermore, during the settling process, their irregular shapes intensify wake interactions between adjacent falling particles. This effect, combined with intense turbulent entrainment at the leading edge of the particle cloud, significantly increases the particle cloud's additional mass and fluid resistance [15]. Consequently, the initial kinetic energy obtained from different air release heights is rapidly dissipated by the enhanced hydrodynamic resistance, causing the velocity evolution trajectory at the leading edge to converge rapidly.

3.3. Front Position

The frontal position (Δx) is an important indicator reflecting the penetration ability of the particle cloud. The release height (H), particle size (D_{50}), and initial aspect ratio (L_0/d_0) are all control variables that can affect it [32,41]. The aspect ratio (L_0/d_0) affects the wake during the settling period and the clustering effect of the particles [39]. Considering the highly irregular shape of coral sand, this study introduces the St to represent the dynamics of a single particle. Figure 8 shows the variation in the normalized front position (x/l) with the modified dimensionless time factor $(t/T)(L_0/d_0)^{0.1}$ [41]. After quantitatively evaluating these data collapses, the coefficients of determination (R^2) for H = 0, 10, and 20 cm were found to be R^2 = 0.79, R^2 = 0.91, and R^2 = 0.84, respectively. For coarse coral sand ($0.33 \leq St < 1$), an increase in the initial aspect ratio (L_0/d_0) has a negligible effect on front evolution (as shown in Figure 8a,b). In contrast, the front displacement of medium- and fine-grained coral sand ($0 < St < 0.33$) exhibits extreme sensitivity to changes in the aspect ratio (as shown in Figure 8c).

In summary, although the current scaling analysis does not examine the individual effects of each variable, it clearly demonstrates that the front position (Δx) is governed by the coupling between particle inertia (St) and aspect ratio (L_0/d_0). Coarse-grained deposition is gravity-dominated, whereas the evolution of medium- and fine-grained particles is highly dependent on the wake aggregation effect caused by the aspect ratio.

Introducing the aspect ratio factor into the dimensionless time establishes a practical and quantitatively supported empirical framework for predicting the spatiotemporal evolution of cloud clusters.

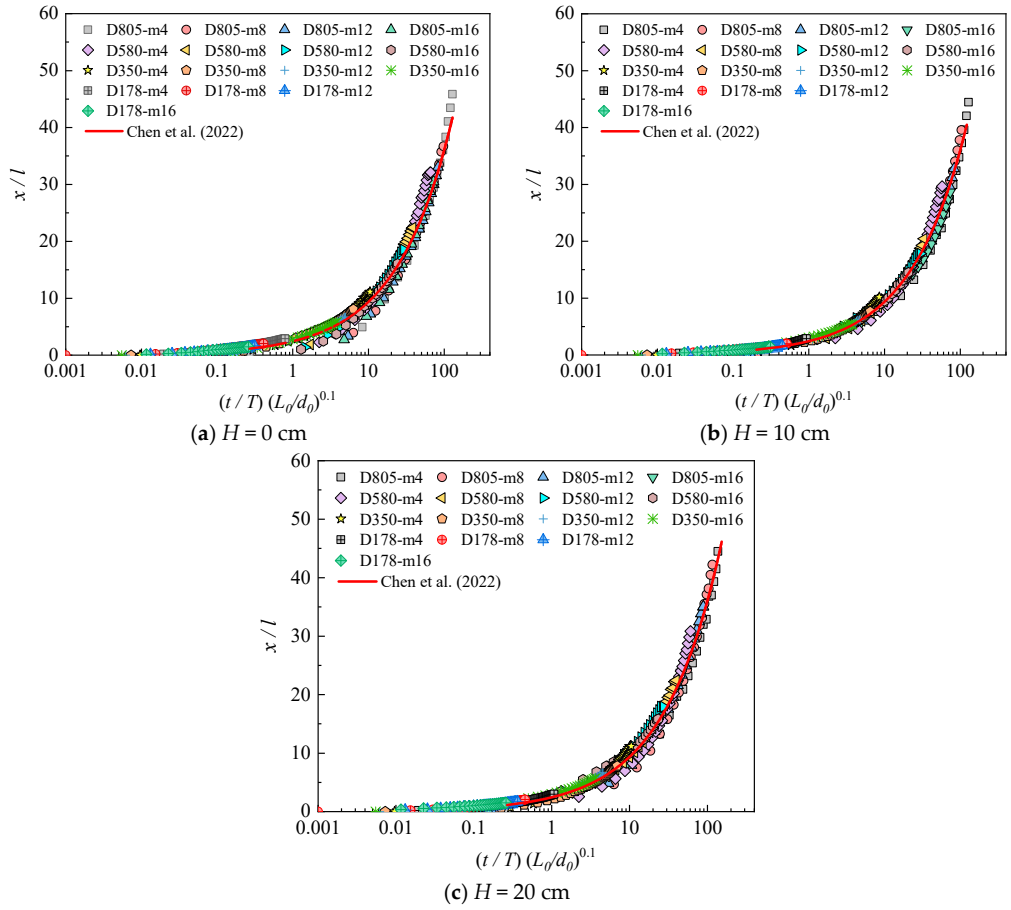


Figure 8. Effect of L_0/d_0 on normalized frontal position x/l with specified normalization times, t/T. (**a**) Results for release height H = 0 cm; (**b**) Results for release height H = 10 cm; (**c**) Results for release height H = 20 cm [41].

3.4. Growth Rate of Width

The normalized diffusion width (b/d_0) is a key parameter for quantifying the lateral expansion of a particle cloud. The air release height (H) controls the impact kinetic energy of the particle cloud upon entry into the water. Based on the laws governing outflow from an orifice and free fall, the initial velocity and impact velocity are defined as $u_0 = c_1(gd_0)^{1/2}$ and $u_i = \sqrt{u_0^2 + 2gH}$ [45], respectively. This study introduces a dimensionless impact parameter ($\eta = u_i/u_0$) to quantify the influence of initial momentum. Given the significant material-specific differences in lateral diffusion between coral sand and conventional quartz sand, Figure 9 compares the width data for coral sand at different release heights with the quartz sand prediction model established by Moghadaripour (Equation (4)) [39].

$$\frac{b}{d_0} = \left\{ \left[0.236 + 0.0029 \left(\frac{L_0}{d_0} \right) \right] - \left(4 \times 10^{-5} \eta^2 + 0.0017 \eta \right) \right\} \left(\frac{x}{d_0} \right) \quad (4)$$

Figure 9 shows the variation in the normalized width (b/d_0) with respect to the normalized depth (x/d_0) at different release heights (H = 0 cm, 10 cm, 20 cm). Based on the St, particles are classified into three size regions [39]: large particles (Figure 9a,b, $0.33 \leq St < 1$): At $x/d_0 < 10$, the effect of release height is negligible. The particle group maintains the initial jet state and follows the predicted jet leading edge. When $x/d_0 > 10$,

lower release heights result in a significant widening of the cloud. Medium particles (Figure 9c,d, $0.1 < St < 0.33$): When the initial aspect ratio is large, the release height has no significant effect on the overall width of the cloud. Small particles (Figure 9e,f, $0 < St \leq 0.1$): When $L_0/d_0 = 3.621$, the difference in width is only significant in the range $8 < x/d_0 < 22$; after exceeding 22, the lateral diffusion trajectories tend to converge. Smaller particles exhibit extremely high sensitivity to environmental vortices.

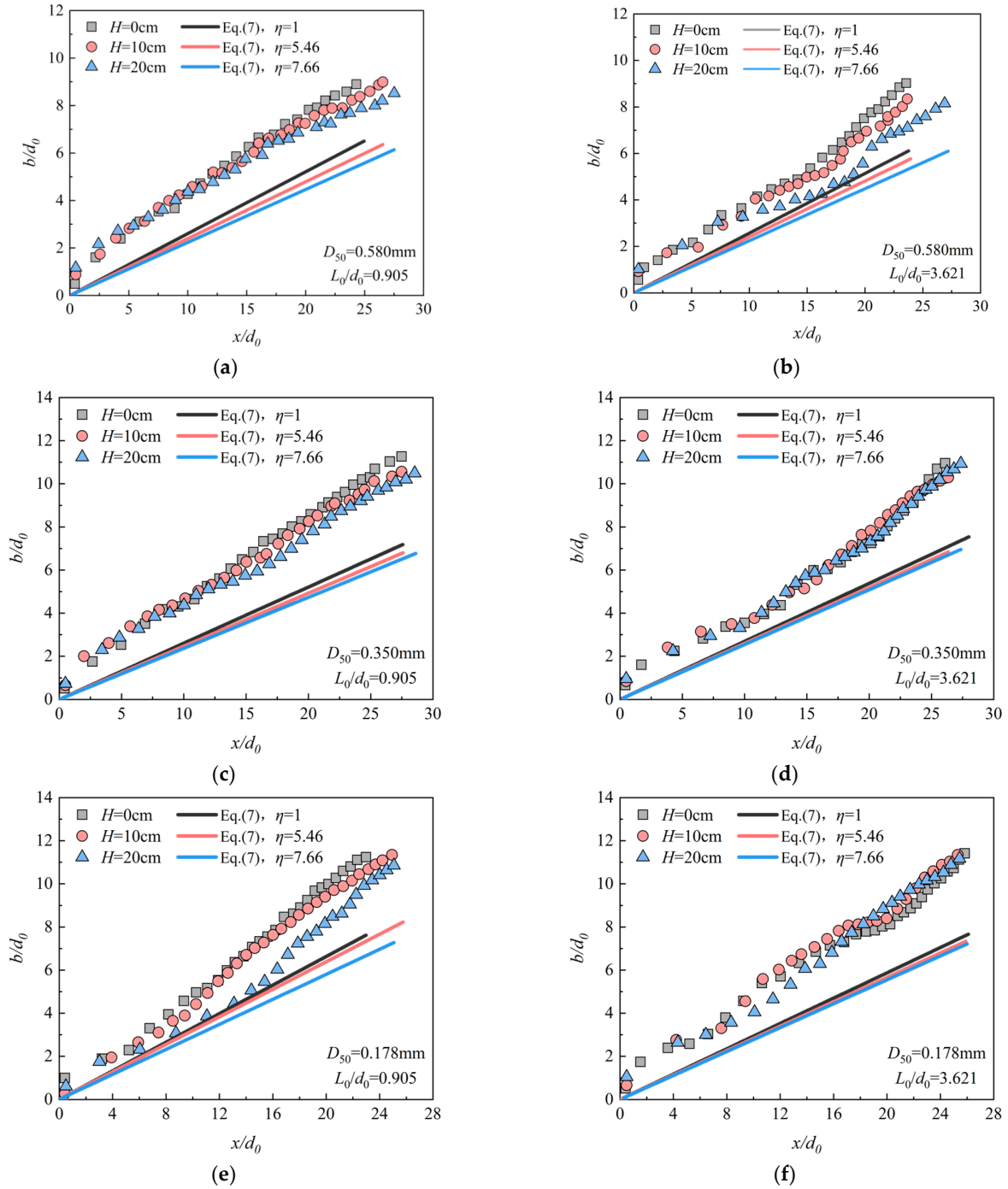


Figure 9. Effect of air release height on normalized width, b/d_0, give a specified normalized depth x/d_0. (**a**,**b**) $0.33 \leq St < 1$; (**c**,**d**) $0.1 < St < 0.33$; (**e**,**f**) $0 < St \leq 0.1$.

As shown in Figure 10, the evolution of particle cloud width over time for different aspect ratios demonstrates a positive correlation between cloud width and aspect ratio. However, when L_0/d_0 is between 2.715 and 3.621, the difference in coral sand cloud width

is very small. In other words, when $L_0/d_0 > 2$, increases L_0/d_0 do not increase the cloud width. A study by Moghadaripour et al. reported similar results [39].

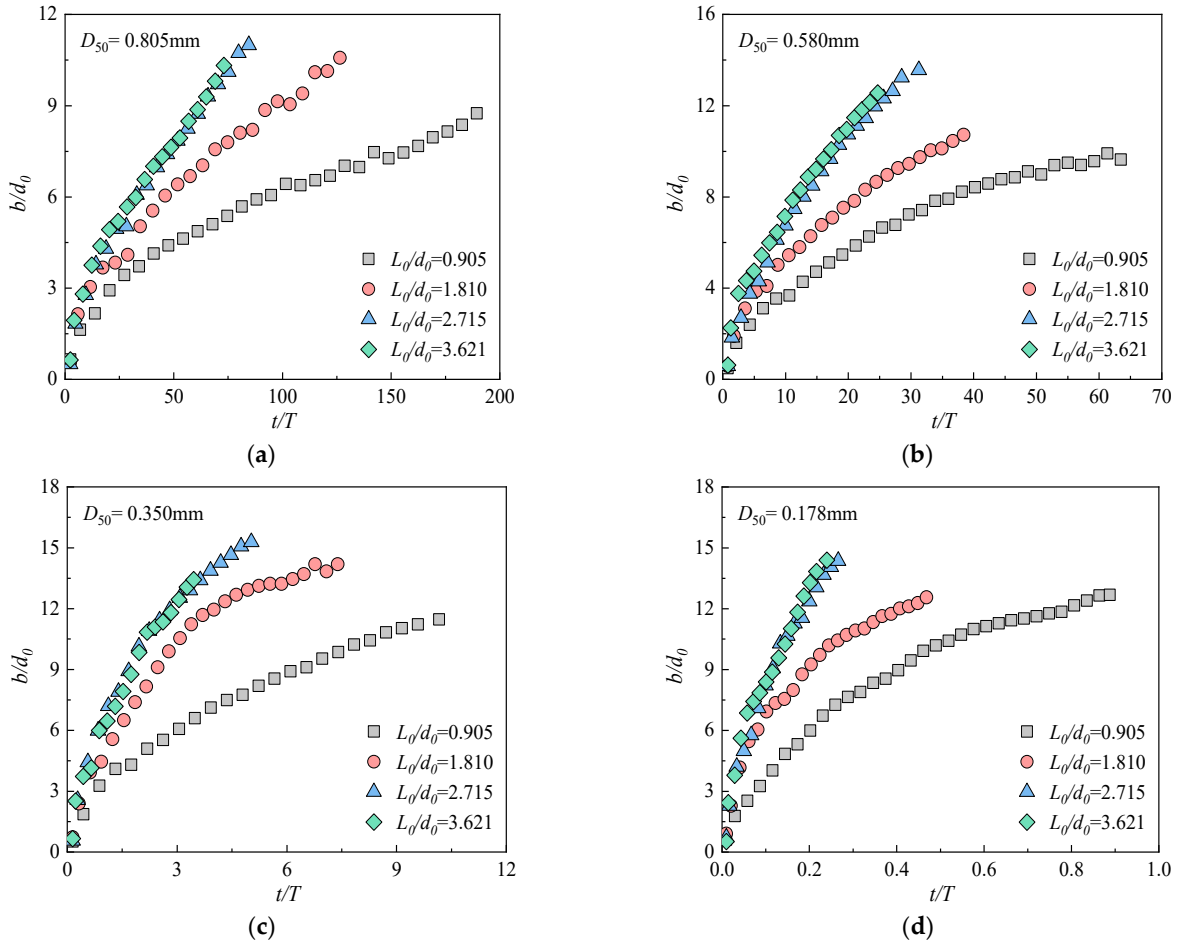


Figure 10. Effect of particle size and aspect ratio on cloud width. (**a**) Results for particle size D_{50} = 0.805 mm; (**b**) Results for particle size D_{50} = 0.580 mm; (**c**) Results for particle size D_{50} = 0.350 mm; (**d**) Results for particle size D_{50} = 0.178 mm.

This study modifies the original prediction equation. It proposes a novel empirical prediction model (Equation (5)) specifically tailored to the unique geometric characteristics of coral sand:

$$\frac{b}{d_0} = 0.89 + \left\{ \left[0.3356 + 0.0069 \left(\frac{L_0}{d_0} \right) \right] - \left(0.004\eta^2 + 0.0084\eta \right) \right\} \left(\frac{x}{d_0} \right) \quad (5)$$

Compared with the quartz sand model (Equation (4)), the empirical model for coral sand proposed in this paper (Equation (5)) incorporates several key modifications. Mathematically, the new model introduces an intercept of 0.89 and increases the coefficients of the aspect ratio (L_0/d_0) and the coefficients of the parameters. In terms of physical mechanisms, these modifications reflect the unique hydrodynamic response characteristics of coral sand. The introduction of the initial intercept (0.89) and the enhancement in the initial motion conditions are attributed to the irregular morphology and porous structure of coral sand, characteristics that significantly increase fluid resistance and wake entrainment during the initial phase when the particle bed enters the water surface.

To demonstrate the effectiveness of the new model, experimental data were substituted into the two equations above for evaluation. As shown in Table 2, compared with Equation (4) (R^2 = 0.64, RMSE = 0.36), Equation (5) yielded a higher coefficient of determi-

nation (R^2 = 0.93) and a lower root mean square error (RMSE = 0.08), providing reliable quantitative validation of its predictive capability. Furthermore, this model has strictly defined valid boundaries: shape factor $0.34 \leq St \leq 0.894$, aspect ratio $0.196 \leq L_0/d_0 \leq 3.621$, and dimensionless impact parameter $1 \leq \eta \leq 7.66$.

Table 2. Quantitative performance metrics of different models.

Predictive Model	R^2	RMSE
Moghadaripour (Equation (4))	0.64	0.36
Proposed Model (Equation (5))	0.93	0.08

3.5. Diffusion Angle

The diffusion angle (θ) is one of the important parameters that affect the diffusion of the particle cloud. The change in this angle is mainly influenced by the release height (H), particle size (D_{50}), and initial aspect ratio (L_0/d_0). Previous studies have shown that the size of the diffusion angle reflects the momentum transfer and mixing degree between the particle group and the still water [39].

Figure 11 reveals the dynamic evolution of the diffusion angle (θ) as a function of the initial aspect ratio (L_0/d_0). For coral sand with large particle sizes ($0.33 \leq St < 1$), increasing L_0/d_0 does not increase the diffusion angle of the particle cloud. As particle size decreases, the diffusion angle of particle clouds with different aspect ratios exhibits fluctuations. These fluctuations are attributed to the fact that smaller particles are more susceptible to the influence of vortices. When $D_{50} \geq 0.580$ mm, a larger aspect ratio results in a smaller entry angle of the particles into the water and a narrower width.

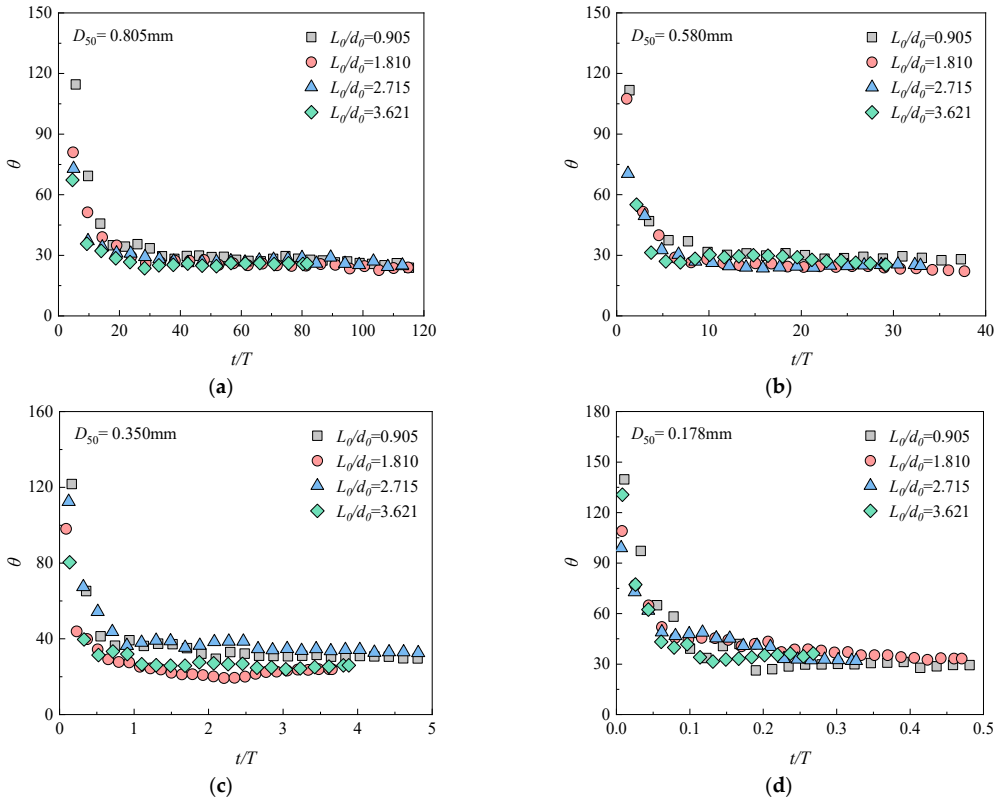


Figure 11. Effect of aspect ratio on diffusion angle θ of particle clouds with different particle sizes. (**a**) Results for particle size D_{50} = 0.805 mm; (**b**) Results for particle size D_{50} = 0.580 mm; (**c**) Results for particle size D_{50} = 0.350 mm; (**d**) Results for particle size D_{50} = 0.178 mm.

Figure 12 illustrates the effect of particle size on the diffusion angle (at a fixed aspect ratio (L_0/d_0 = 1.810). Particle clouds composed of medium- to large-sized particles ($0.1 < St < 0.33$ and $0.33 \leq St < 1$) exhibit similar diffusion angles. In contrast, particle clouds composed of finer particles ($0 < St \leq 0.1$) exhibit larger diffusion angles.

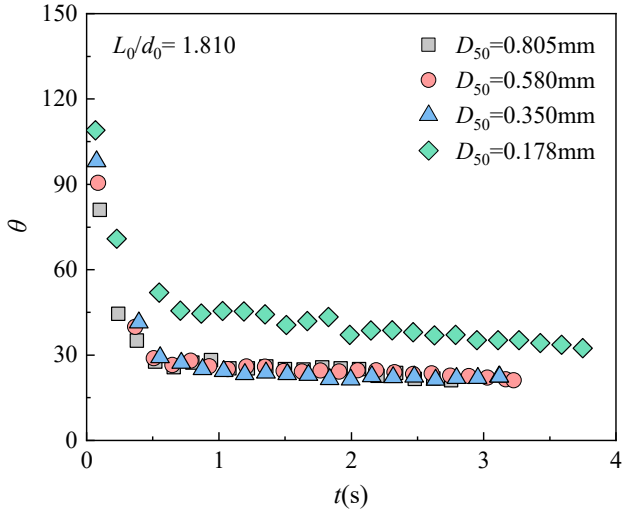
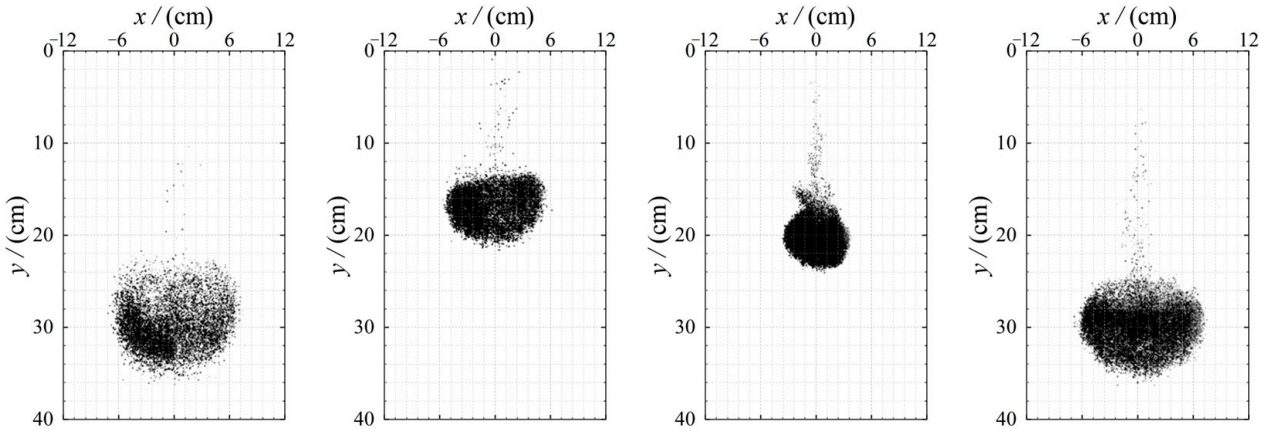


Figure 12. L_0/d_0 = 1.810, the effect of particle size on the diffusion angle θ of the particle cloud.

Figure 13 illustrates the morphological evolution of particle clouds at different release heights H. Figure 14 provides a further quantitative analysis of the effect of release height on the spreading angle (θ), excluding the initial sandblasting phase. Figure 14 shows that an increase in release height leads to a decrease in the diffusion angle (θ). The more elongated and compact cloud profiles observed at higher release heights in Figure 13 corroborate this trend. Based on the observed particle cloud profiles, we speculate that the extremely high initial impulse upon entry into the water may have enhanced the particles' vertical penetration capability. This enhanced downward impulse may, in turn, have suppressed the lateral turbulent diffusion of the cloud. However, this study does not include direct measurements of turbulence, entrainment, or internal flow field characteristics. Therefore, the physical mechanisms described above are currently only reasonable inferences based on macroscopic evolutionary features and still require direct flow field data for confirmation.



(**a**) H = 0 cm, D_{50} = 0.805 mm, t^* = 10 and t^* = 20 (**b**) H = 0 cm, D_{50} = 0.580 mm, t^* = 10 and t^* = 20

Figure 13. *Cont.*

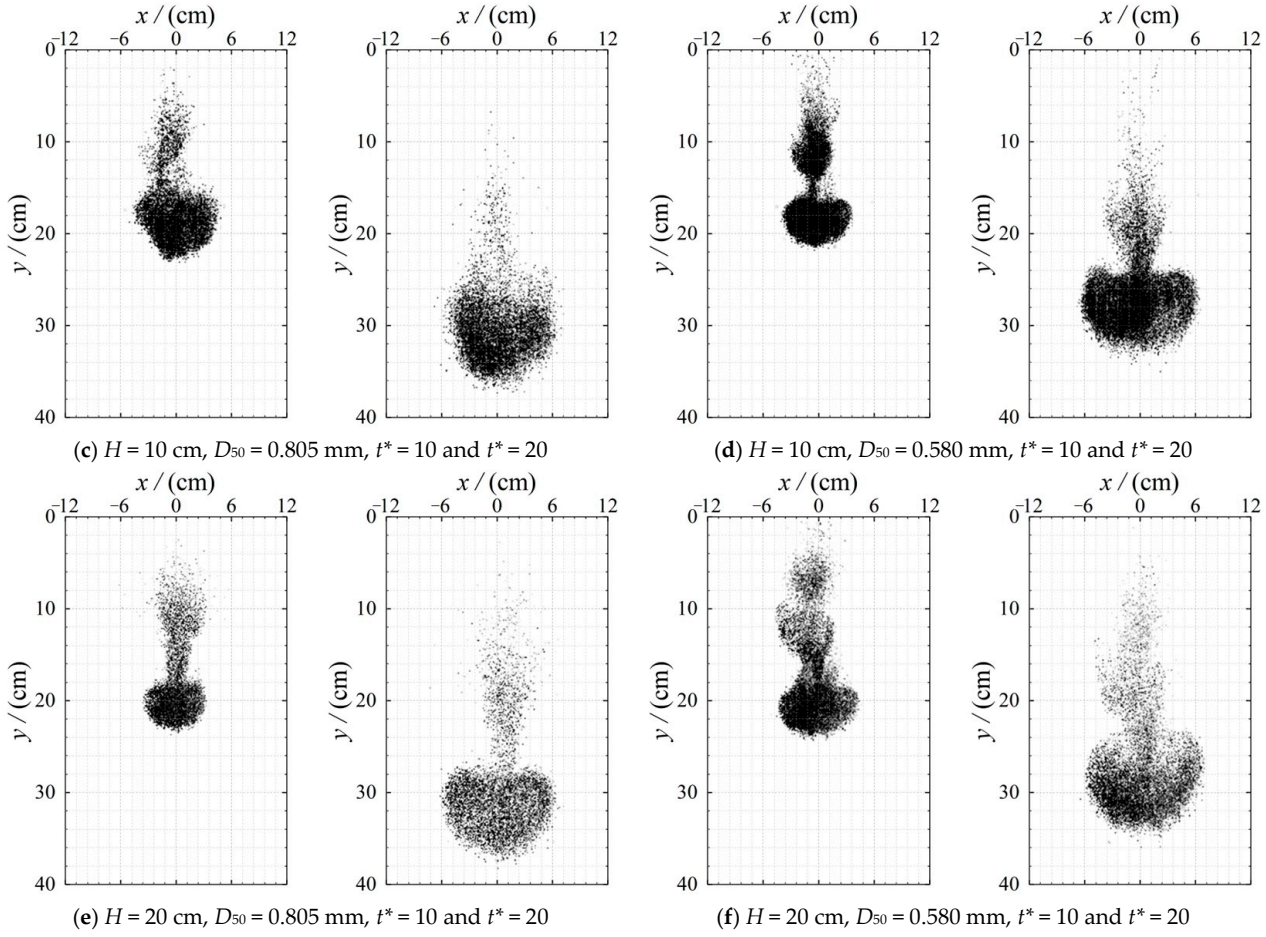


Figure 13. Evolution of particle clouds with d_0 = 15 mm and m = 8 g at different air release heights.

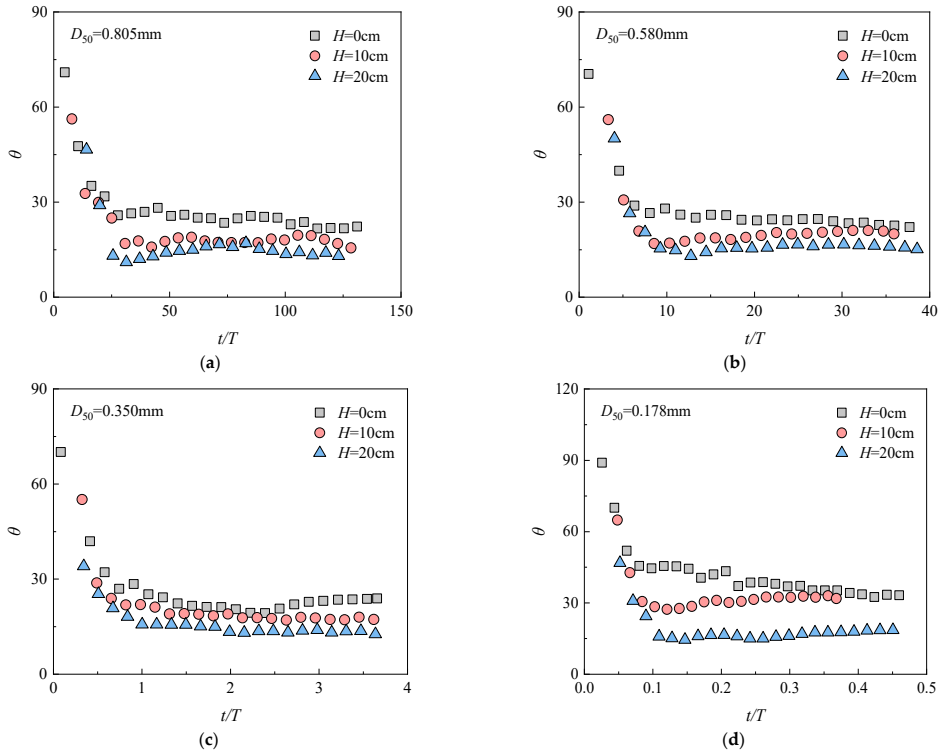


Figure 14. Effect of air release height on the diffusion angle θ of particle clouds. (**a**) Results for particle size D_{50} = 0.805 mm; (**b**) Results for particle size D_{50} = 0.580 mm; (**c**) Results for particle size D_{50} = 0.350 mm; (**d**) Results for particle size D_{50} = 0.178 mm.

The dispersion angle of coral sand plumes is primarily influenced by a combination of particle size, intrinsic morphology (such as aspect ratio), and release height. Particle size and morphology in natural coral sand typically vary in tandem. Therefore, within the existing experimental framework, the independent contribution of particle morphology cannot be completely decoupled from the effects of particle size. Nevertheless, both an increase in overall particle size and an increase in release height significantly reduce the diffusion angle. This phenomenon effectively suppresses the lateral expansion of the plume. The coupled action of these mechanisms ultimately determines the spatial distribution boundaries of submerged sediments.

3.6. Diffusion Coefficient

The diffusion coefficient (ε) governs the random diffusion and mass transport of suspended particles [47]. In this study, the release of coral sand is approximated using an instantaneous point source model [48]. To derive the effective diffusion coefficient of coral sand in a two-dimensional plane under specific experimental boundary conditions, we start from the generalized three-dimensional diffusion governing equation [49]:

$$\frac{\partial C}{\partial t} = D\left(\frac{\partial^2 C}{\partial x^2} + \frac{\partial^2 C}{\partial y^2} + \frac{\partial^2 C}{\partial z^2}\right) \tag{6}$$

To isolate the core dispersion mechanism and simplify the analytical solution, we define the boundary and initial conditions using the Dirac function and solve for the one-dimensional diffusion case:

$$C(\pm\infty, t) = 0, C(x, 0) = (m / A)\delta(x) \tag{7}$$

where m is the total mass, and A is the cross-sectional area. By introducing the Boltzmann transformation, we can obtain the analytical solution for the Gaussian distribution in the one-dimensional case.

For two-dimensional planar transport, the spatial integral (C) of the concentration over the control volume v is equal to the total mass (m) [50]:

$$\int_v c(x, y)dv = \int_{x_0}^{x_n}\int_{y_0}^{y_n} \frac{m}{\mu\sqrt{4\pi\varepsilon x/\mu}} exp\left(-\frac{y^2\mu}{4\varepsilon x} - \frac{w_s x}{h\mu}\right)dxdy = m \tag{8}$$

In the equation, μ represents the average horizontal advection velocity, w_s represents the sedimentation velocity, and h represents the water depth. To simplify the integration of the complex exponential term, this study performs a Taylor series expansion of the first two terms. This numerical approximation restricts the solution to the near-field dispersion region:

$$\sqrt{4\pi\varepsilon\mu} = \int_{x_0}^{x_n}\left[\sqrt{0.4} - \frac{2}{3}\times 10^{-\frac{1}{3}}\left(\frac{\varepsilon x}{\mu}\right)^{\frac{1}{6}}\right] x^{-\frac{1}{2}} e^{\frac{w_s x}{n\mu}} dx \tag{9}$$

The geometric boundary and kinematic parameters obtained from the flume experiments are shown in Table 3.

Table 3. The values of the relevant parameters.

Parameters	x_0 (m)	x_n (m)	y_0 (m)	y_n (m)	h (m)	m (kg)	μ (m/s)	w_s (m/s)
Value	−0.12	0.12	−0.12	0.12	0.8	0.4×10^{-3}	0.1	0.15

After substituting the experimental parameters into the integral equation, the diffusion coefficient of the coral sand was determined as follows:

$$\varepsilon = 0.44 \tag{10}$$

Notably, the derived value of this diffusion coefficient is based on calculations under the current experimental conditions. This value is not applicable to all scenarios. Theoretically, truncating the first two terms of the Taylor series is reasonable in the near-field diffusion region. Within this region, higher-order terms decay rapidly. However, applying this approach to far-field scenarios will inevitably introduce errors. Such errors may lead to an underestimation of far-field diffusion dynamics. Furthermore, this estimated value is inherently sensitive to initial kinematic parameters (such as sedimentation rate and water depth). Therefore, while this estimate performs robustly under the boundary conditions specified in Table 3, its general applicability in broader hydrodynamic environments remains to be verified. Future applications will require rigorous uncertainty and parameter sensitivity analyses.

From this, the final analytical equation for the concentration of coral sand in a two-dimensional plane was derived:

$$c(x,y) = \frac{m}{\sqrt{1.76\pi x\mu}} exp(-\frac{y^2\mu}{1.76\varepsilon x} - \frac{w_s x}{h\mu}) \tag{11}$$

Although the diffusion coefficients of coral sand and quartz sand differ significantly [45], their concentration trends over time are basically similar, both following an exponential function form. Figure 9 can further prove this conclusion. Although they exhibit similarities in this regard, this does not mean that their entire dynamic evolution process is exactly the same. The underlying control mechanisms—particularly the local hydrodynamic behavior influenced by the irregular morphology of coral sand—may still exhibit different dynamic characteristics compared to typical quartz sand.

4. Discussion

This study systematically investigates the dynamical mechanisms and evolution of coral sand clouds. Although previous research has extensively studied the evolution of particle clouds (e.g., Moghadaripour et al.'s work [39] on quartz sand), studies specifically focused on coral sand particle clouds remain insufficiently systematic. Although Chen et al. [51] conducted preliminary observations of coral sand clouds, they did not provide a standardized definition of the formation stages of these clouds. To address this critical gap, this study quantitatively examined the evolution of coral sand clouds by introducing a dimensionless time parameter and established a systematic framework. Additionally, this study systematically analyzed the coupled effects of the initial aspect ratio (L_0/d_0), release height (H), and Stokes number (St).

Most existing studies on the complex hydrodynamic behavior of coral sand have focused on single particles. For example, a series of studies by Bian et al. [52,53] demonstrated that the threshold velocities for coral sand particles to begin movement under steady flow and oscillating wave currents are entirely different from those of quartz sand. However, the kinematic characteristics of single particles cannot be directly applied to the evolution of macroscopic particle clouds. There is a gap in systematic research on particle clouds. This paper systematically analyzes the coupled effects of initial aspect ratio, release height, and Stokes number. The results clearly reveal the control mechanisms by which microscopic morphological characteristics govern macroscopic dispersion. It should be noted that the

proposed interpretations apply specifically to natural coral sand systems, where particle size and morphology are inherently coupled.

The particle clouds observed in the experiments and existing literature [43,45,54] indicate that surface instabilities and the formation of impact craters dissipate the excess kinetic energy generated by the release height. At the same time, vortices draw air into the water, creating an upward motion that slows the downward velocity of the particles. However, the release height alters the lateral width of the sand jet and the particle cloud [43,55]. As the release height increases, the initial acceleration time of the particle cloud in water decreases, but its growth rate in the second stage remains constant [56]. For particles with moderate Stokes numbers ($0.1 < St < 1$), an increase in release height enhances the wake effects during the transient process (see Figure 13). This enhanced wake causes the volume of the main particle plume to shrink and reduces the diffusion width and diffusion angle (see Figures 9a–c and 14a–c). In contrast, for fine particles ($0 < St \leq 0.1$), vortex structures dominate, causing the particles to fully follow the motion of the surrounding fluid. In the absence of direct turbulence and internal entrainment data, these mechanisms are merely macroscopic inferences and still require verification with future flow field data.

The proposed empirical formula (Equation (5)) and the calculated diffusion coefficient ($\varepsilon = 0.44$) quantify different aspects of coral sand plume evolution, respectively. Empirical Formula (5) directly predicts the diffusion width of the coral sand plume. This formula reflects the drag effects caused by irregular particles through empirical coefficients. So, there is no need to introduce additional complex morphological parameters in the calculations. On the other hand, the diffusion coefficient ($\varepsilon = 0.44$) can be used to directly assess sediment transport in the near-field waters. Marine engineering operations (such as dredging, land reclamation, and seabed mining) rely on accurate predictions of the aforementioned diffusion width and transport scale to control ecological impacts on surrounding coral reefs [57,58]. These independent near-field parameters provide foundational inputs for far-field numerical modeling and environmental assessments.

5. Conclusions

This study investigates the evolution mechanisms of coral sand particle clouds in water through systematic flume experiments, leading to the following conclusions:

Elucidating macroscopic hydrodynamic mechanisms: Based on a dimensionless time scale ($t^* = t/T$), this study divides the evolution of a particle cloud into distinct phases: $t^* \leq 1$ dominated the initial sand blasting acceleration stage, and $1 < t^* \leq 12$ corresponds to the transient phase, which is macroscopically characterized by a prominent wake. Furthermore, the highly irregular morphology of coral sand is a key factor contributing to its significantly different motion characteristics, resulting in macroscopic behavior that differs markedly from that of typical quartz sand.

Establishing a multivariate coupling framework: Macroevolution is governed by the coupling of multiple initial control variables, including the initial aspect ratio (L_0/d_0), Stokes number (St), and release height (H). Specifically, when $1 \leq \eta \leq 7.66$, the release height (H) has no significant effect on the front velocity (u_f) or position. A higher release height (H) results in a narrower front and a smaller diffusion angle.

Developing an empirical prediction model: Based on experimental results, an empirical formula was established, and the diffusion coefficient of coral sand was calculated. The empirical formula can be used to predict the diffusion width of coral sand; its coefficient implicitly accounts for shape-induced resistance. At the same time, the diffusion coefficient ($\varepsilon = 0.44$) directly reflects the intensity of near-field propagation.

In summary, this study characterizes the evolutionary characteristics of coral sand plumes and evaluates the coupled effects of various controlling variables on these plumes.

These findings contribute to understanding the kinematic properties of coral sand and the implementation of marine engineering projects. However, the empirical models and diffusion coefficients currently proposed are limited to specific hydrostatic laboratory conditions. Future research should incorporate flow field measurements and hydrodynamic environments to validate and extend these near-field findings, making them applicable to complex far-field dispersion scenarios.

Author Contributions: Conceptualization, J.C. and F.L.; methodology, F.L. and X.L.; software, X.L.; validation, F.L. and X.L.; formal analysis, Z.Y.; investigation, J.C.; resources, J.C. and C.J.; data curation, X.L. and F.L.; writing—original draft preparation, X.L. and F.L.; writing—review and editing, J.C., F.L. and C.J.; visualization, Z.W.; supervision, J.C. and Z.W.; project administration, J.C. and Z.W.; funding acquisition, J.C. and F.L. All authors have read and agreed to the published version of the manuscript.

Funding: This research was funded by the National Natural Science Foundation of China (Grant No. 52271257) and Research Innovation Project for Graduate students in Hunan Province (Grant No.CX20210821). The APC was funded by Jie Chen.

Data Availability Statement: The data are available from the corresponding author upon reasonable request.

Conflicts of Interest: The authors declare no conflicts of interest.

References

1. Asaoka, S.; Jadoon, W.A.; Umehara, A.; Takeda, K.; Otani, S.; Ohno, M.; Fujitake, N.; Sakugawa, H.; Okamura, H. Organic matter degradation characteristics of coastal marine sediments collected from the Seto Inland Sea, Japan. *Mar. Chem.* **2020**, *225*, 103854. [CrossRef]
2. Piecuch, C.G.; Calafat, F.M.; Dangendorf, S.; Jordà, G. The ability of barotropic models to simulate historical mean sea level changes from coastal tide gauge data. *Surv. Geophys.* **2019**, *40*, 1399–1435. [CrossRef]
3. Liu, B.; Wang, J.; Xu, M.; Wang, Z.; Zhao, L. Evaluation of the comprehensive benefit of various marine exploitation activities in China. *Mar. Policy* **2020**, *116*, 103924. [CrossRef]
4. He, S.H.; Shan, H.F.; Xia, T.D.; Liu, Z.J.; Ding, Z.; Xia, F. The effect of temperature on the drained shear behavior of calcareous sand. *Acta Geotech.* **2021**, *16*, 613–633.
5. Hora, C.; Caldwell, I.R.; Birkeland, C.; McManus, J.W. Dredging in the Spratly Islands: Gaining land but losing reefs. *PLoS Biol.* **2016**, *14*, e1002422. [CrossRef]
6. McManus, J.W. Offshore coral reef damage, overfishing, and paths to peace in the South China Sea. *Int. J. Mar. Coast. Law* **2017**, *32*, 199–237. [CrossRef]
7. Lisi, I.; Feola, A.; Bruschi, A.; Pedroncini, A.; Pasquali, D.; Di Risio, M. Mathematical modeling framework of physical effects induced by sediments handling operations in marine and coastal areas. *J. Mar. Sci. Eng.* **2019**, *7*, 149. [CrossRef]
8. Xu, L.; Li, X.; Yajiao, L.; Zhichao, H. Numerical Simulation of Sediment Plume Dispersion in Deep-Sea Mining Areas Based on the Similarity Principle. *J. Mar. Sci. Eng.* **2026**, *14*, 673. [CrossRef]
9. Gensheimer, R.J.; Adams, E.E.; Law, A.W. Dynamics of particle clouds in ambient currents with application to open-water sediment disposal. *J. Hydraul. Eng.* **2013**, *139*, 114–123. [CrossRef]
10. Ding, W.; Lu, C.; Xie, Q.; Luo, X.; Zhang, G. Understanding the settling processes of dredged sediment disposed in open waters through experimental tests and numerical simulations. *J. Mar. Sci. Eng.* **2022**, *10*, 220. [CrossRef]
11. Kriaa, Q.; Subra, E.; Favier, B.; Le Bars, M. Effects of particle size and background rotation on the settling of particle clouds. *Phys. Rev. Fluids* **2022**, *7*, 124302. [CrossRef]
12. Ouillon, R.; Meiburg, E.; Sutherland, B.R. Turbidity currents propagating down a slope into a stratified saline ambient fluid. *Environ. Fluid Mech.* **2019**, *19*, 1143–1166. [CrossRef]
13. Necker, F.; Härtel, C.; Kleiser, L.; Meiburg, E. High-resolution simulations of particle-driven gravity currents. *Int. J. Multiph. Flow.* **2002**, *28*, 279–300.
14. Maragos, J.E. Impact of coastal construction on coral reefs in the US-affiliated pacific Islands. *Coast. Manag.* **1993**, *21*, 235–269. [CrossRef]
15. Noh, Y.; Fernando, H.J.S. The transition in the sedimentation pattern of a particle cloud. *Phys. Fluids A Fluid Dyn.* **1993**, *5*, 3049–3055. [CrossRef]
16. Rahimipour, H.; Wilkinson, D. Dynamic behavior of particle clouds. In *Proceedings of the 11th Australasian Fluid Mechanics Conference*; Australasian Fluid Mechanics Society: Hobart, Australia, 1992; pp. 743–746.

17. Sheng, C.; Jiao, J.J.; Xu, H.; Liu, Y.; Luo, X. Influence of land reclamation on fresh groundwater lenses in oceanic islands: Laboratory and numerical validation. *Water Resour. Res.* **2021**, *57*, e2021WR030238. [CrossRef]
18. Ruggaber, G.J. Dynamics of Particle Clouds Related to Open-Water Sediment Disposal. Ph.D. Thesis, Massachusetts Institute of Technology, Cambridge, MA, USA, 2000.
19. Wang, C.; Ding, X.; Yin, Z.Y.; Peng, Y.; Chen, Z. Mechanical characteristics and particle breakage of coral sand under one-dimensional repeated loading. *Acta Geotech.* **2022**, *17*, 3117–3130.
20. Gao, R.; Ye, J. Mechanical behaviors of coral sand and relationship between particle breakage and plastic work. *Eng. Geol.* **2023**, *316*, 107063. [CrossRef]
21. Zingg, T. Beitrag zur Schotteranalyse. Ph.D. Thesis, ETH Zurich, Zurich, Switzerland, 1935.
22. Coop, M.R. The mechanics of uncemented carbonate sands. *Géotechnique* **1990**, *40*, 607–626. [CrossRef]
23. Wang, X.; Wu, Y.; Cui, J.; Zhu, C.Q.; Wang, X.Z. Shape characteristics of coral sand from the South China Sea. *J. Mar. Sci. Eng.* **2020**, *8*, 803. [CrossRef]
24. Tong, C.X.; Burton, G.J.; Zhang, S.; Sheng, D. Particle breakage of uniformly graded carbonate sands in dry/wet condition subjected to compression/shear tests. *Acta Geotech.* **2020**, *15*, 2379–2394.
25. Mao, L.; Li, J.; Shimozono, T.; Tajima, Y. Impacts of particle shape, skeletal porosity and density on the settling velocity of gravel-size coral debris. *J. Geophys. Res. Earth Surf.* **2023**, *128*, e2022JF006996. [CrossRef]
26. Wang, A.; Xu, Z.; Chu, Y.; Dai, J.G.; Xu, Q.; Liu, K.; Ding, Y.; Sun, D. Numerical characterization of the geometric shape of coral sand by particle shaping and study on the properties of graded composite coral fine aggregate. *Compos. Part B Eng.* **2025**, *297*, 112313. [CrossRef]
27. Ting, J.M.; Meachum, L.; Rowell, J.D. Effect of particle shape on the strength and deformation mechanisms of ellipse-shaped granular assemblages. *Eng. Comput.* **1995**, *12*, 99–108.
28. Rousé, P.C.; Fannin, R.J.; Shuttle, D.A. Influence of roundness on the void ratio and strength of uniform sand. *Géotechnique* **2008**, *58*, 227–231. [CrossRef]
29. Liu, Q.B.; Xiang, W.; Lehane, B.; Cui, D.; Li, Y. Experimental study of effect of particle shapes on shear strength of sand and tip resistance of driven piles. *Chin. J. Rock Mech. Eng.* **2011**, *30*, 400–410.
30. Payan, M.; Khoshghalb, A.; Senetakis, K.; Khalili, N. Effect of particle shape and validity of Gmax models for sand: A critical review and a new expression. *Comput. Geotech.* **2016**, *72*, 28–41. [CrossRef]
31. Kandasami, R.K.; Murthy, T.G. Manifestation of particle morphology on the mechanical behaviour of granular ensembles. *Granul. Matter* **2017**, *19*, 21. [CrossRef]
32. Azimi, A.H.; Zhu, D.Z.; Rajaratnam, N. Computational investigation of vertical slurry jets in water. *Int. J. Multiph. Flow* **2012**, *47*, 94–114. [CrossRef]
33. Sharif, F.; Azimi, A.H. Particle cloud dynamics in stagnant water. *Int. J. Multiph. Flow* **2020**, *125*, 103197. [CrossRef]
34. Janati, M.; Azimi, A.H. Mixing of twin particle clouds in stagnant water. *J. Eng. Mech.* **2021**, *147*, 04021022. [CrossRef]
35. Sabershahraki, M.; Azimi, A.H. On Dynamics of Sand Particles Impinging Into an Oil Layer by Two Adjacent Nozzles. *J. Fluids Eng.* **2026**, *148*, 011403.
36. Lau, T.C.; Nathan, G.J. The influence of Stokes number on particle clustering within a two-phase turbulent jet. In *Proceedings of the 7th Australian Conference on Laser Diagnostics in Fluid Mechanics and Combustion*; Monash University: Melbourne, Australia, 2015.
37. Li, H.; Ali, W.; Chassagne, C.; Botto, L. Estimating the density of individual particles from the settling of a particle cloud. *Front. Earth Sci.* **2025**, *13*, 1710847. [CrossRef]
38. Hu, W.; Liu, Y.; Li, S.; Qu, J.; Wang, J. Experimental Investigation on the Settling Velocity and Drag Coefficient of Irregularly Shaped Coral Particles. *J. Hydraul. Eng.* **2025**, *151*, 04025029. [CrossRef]
39. Moghadaripour, M.; Azimi, A.H.; Elyasi, S. Experimental study of particle clouds in stagnant water. *J. Eng. Mech.* **2017**, *143*, 04017082. [CrossRef]
40. Jähne, B. *Digital Image Processing*; Springer: Berlin/Heidelberg, Germany, 2005.
41. Chen, J.; Yao, Z.; Jiang, C.B.; Wu, Z.Y.; Deng, B.; Long, Y.N.; Bian, C. Experiment study of the evolution of coral sand particle clouds in water. *China Ocean. Eng.* **2022**, *36*, 720–733. [CrossRef]
42. Qu, X.L.; Khezzar, L.; Danciu, D.; Labois, M.; Lakehal, D. Characterization of plunging liquid jets: A combined experimental and numerical investigation. *Int. J. Multiph. Flow.* **2011**, *37*, 722–731. [CrossRef]
43. Hall, N.; Elenany, M.; Zhu, D.Z.; Rajaratnam, N. Experimental study of sand and slurry jets in water. *J. Hydraul. Eng.* **2010**, *136*, 727–738. [CrossRef]
44. Bühler, J.; Papantoniou, D.A. On the motion of suspension thermals and particle swarms. *J. Hydraul. Res.* **2001**, *39*, 643–653. [CrossRef]
45. Cai, J.; Hall, N.; Elenany, M.; Zhu, D.Z.; Rajaratnam, N. Observations on sand jets in air. *J. Eng. Mech.* **2010**, *136*, 1181–1186. [CrossRef]
46. Bagheri, G.; Bonadonna, C. On the drag of freely falling non-spherical particles. *Powder Technol.* **2016**, *301*, 526–544. [CrossRef]

47. Fischer, H.B. *Mixing in Inland and Coastal Waters*; Academic Press: Cambridge, MA, USA, 1979.
48. Crank, J. *The Mathematics of Diffusion*; Oxford University Press: Oxford, UK, 1979.
49. Shen, J.; Dongsheng, X.U.; Liu, Z.; Wei, H. Effect of particle characteristics stress on the mechanical properties of cement mortar with coral sand. *Constr. Build. Mater.* **2020**, *260*, 119836. [CrossRef]
50. Lai, A.C.; Zhao, B.; Law, A.W.K.; Adams, E.E. Two-phase modeling of sediment clouds. *Environ. Fluid Mech.* **2013**, *13*, 435–463. [CrossRef]
51. Chen, J.; Yao, Z.; He, F.; Jiang, C.; Jiang, C.; Wu, Z.; Deng, B.; Long, Y.; Bian, C. Experimental study on the settling motion of coral grains in still water. *J. Fluid Mech.* **2024**, *990*, A15. [CrossRef]
52. Bian, C.; Chen, J.; Jiang, C.; Wu, Z.; Yao, Z. Threshold of motion of coral reef sediment under currents in flume experiments. *Sedimentology* **2023**, *70*, 1723–1740. [CrossRef]
53. Bian, C.; Chen, J.; Jiang, C.; Wu, Z.; Yao, Z.; Liu, J. Experimental study of the incipient motion threshold of coral sediment for oscillatory flow. *Ocean Eng.* **2023**, *278*, 114375. [CrossRef]
54. Dissanayake, A.L.; Gros, J.; Socolofsky, S.A. Integral models for bubble, droplet, and multiphase plume dynamics in stratification and crossflow. *Environ. Fluid Mech.* **2018**, *18*, 1167–1202. [CrossRef]
55. Bond, D.; Johari, H. Effects of initial geometry on the development of thermals. *Exp. Fluid* **2005**, *39*, 591–601. [CrossRef]
56. Yu, X.; Chen, L.; Fang, Q.; Zhang, J.; Guo, D.; Hou, X. Determination of attenuation effects of coral sand on the propagation of impact-induced stress wave. *Int. J. Impact Eng.* **2019**, *125*, 63–82. [CrossRef]
57. Dong, Y.; Fu, D.; Feng, X. Engineering Properties of Marine Soils and Offshore Foundations. *J. Mar. Sci. Eng.* **2024**, *12*, 2077. [CrossRef]
58. Tuttle, L.J.; Donahue, M.J. Effects of sediment exposure on corals: A systematic review of experimental studies. *Environ. Evid.* **2022**, *11*, 4. [CrossRef] [PubMed]

Disclaimer/Publisher's Note: The statements, opinions and data contained in all publications are solely those of the individual author(s) and contributor(s) and not of MDPI and/or the editor(s). MDPI and/or the editor(s) disclaim responsibility for any injury to people or property resulting from any ideas, methods, instructions or products referred to in the content.